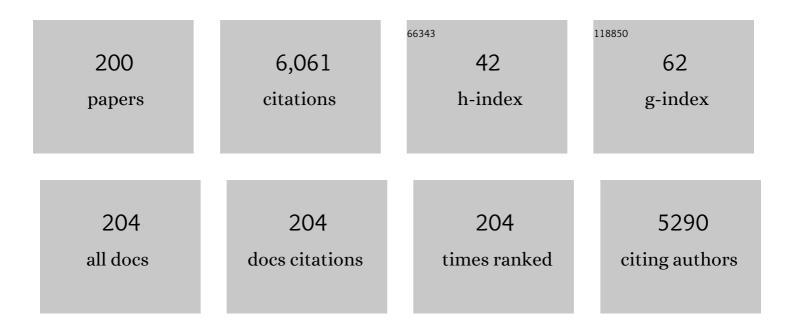
List of Publications by Year in descending order

Source: https://exaly.com/author-pdf/3879083/publications.pdf Version: 2024-02-01



#	Article	IF	CITATIONS
1	Natural grassland as the optimal pattern of vegetation restoration in arid and semi-arid regions: Evidence from nutrient limitation of soil microbes. Science of the Total Environment, 2019, 648, 388-397.	8.0	164
2	Sorption behavior of heavy metals on birnessite: Relationship with its Mn average oxidation state and implications for types of sorption sites. Chemical Geology, 2012, 292-293, 25-34.	3.3	157
3	Characteristics of Phosphate Adsorption-Desorption Onto Ferrihydrite. Soil Science, 2013, 178, 1-11.	0.9	155
4	Lead Binding to Soil Fulvic and Humic Acids: NICA-Donnan Modeling and XAFS Spectroscopy. Environmental Science & Technology, 2013, 47, 11634-11642.	10.0	114
5	Improved removal capacity of magnetite for Cr(VI) by electrochemical reduction. Journal of Hazardous Materials, 2019, 374, 26-34.	12.4	108
6	Patterns of soil microbial nutrient limitations and their roles in the variation of soil organic carbon across a precipitation gradient in an arid and semi-arid region. Science of the Total Environment, 2019, 658, 1440-1451.	8.0	108
7	Mechanisms of soil humic acid adsorption onto montmorillonite and kaolinite. Journal of Colloid and Interface Science, 2017, 504, 457-467.	9.4	104
8	Mechanisms of Mn(II) catalytic oxidation on ferrihydrite surfaces and the formation of manganese (oxyhydr)oxides. Geochimica Et Cosmochimica Acta, 2017, 211, 79-96.	3.9	100
9	As(III) adsorption on Fe-Mn binary oxides: Are Fe and Mn oxides synergistic or antagonistic for arsenic removal?. Chemical Engineering Journal, 2020, 389, 124470.	12.7	98
10	Effect of different vegetation cover on the vertical distribution of soil organic and inorganic carbon in the Zhifanggou Watershed on the loess plateau. Catena, 2016, 139, 191-198.	5.0	97
11	Soil inorganic carbon stock under different soil types and land uses on the Loess Plateau region of China. Catena, 2014, 121, 22-30.	5.0	92
12	Arbuscular mycorrhizal mycelial networks and glomalin-related soil protein increase soil aggregation in Calcaric Regosol under well-watered and drought stress conditions. Soil and Tillage Research, 2019, 185, 1-8.	5.6	85
13	Remediation of heavy metal contaminated soils by organic acid extraction and electrochemical adsorption. Environmental Pollution, 2020, 264, 114745.	7.5	85
14	Adsorption and redox reactions of heavy metals on Fe–Mn nodules from Chinese soils. Journal of Colloid and Interface Science, 2005, 284, 600-605.	9.4	83
15	Characterization of Ni-rich hexagonal birnessite and its geochemical effects on aqueous Pb2+/Zn2+ and As(III). Geochimica Et Cosmochimica Acta, 2012, 93, 47-62.	3.9	83
16	The associations of heavy metals with crystalline iron oxides in the polluted soils around the mining areas in Guangdong Province, China. Chemosphere, 2016, 161, 181-189.	8.2	82
17	Interaction between Humic Acid and Lysozyme, Studied by Dynamic Light Scattering and Isothermal Titration Calorimetry. Environmental Science & Technology, 2009, 43, 591-596.	10.0	75
18	Surface properties and phosphate adsorption of binary systems containing goethite and kaolinite. Geoderma, 2014, 213, 478-484.	5.1	74

#	Article	IF	CITATIONS
19	Relationship Between Pb ²⁺ Adsorption and Average Mn Oxidation State in Synthetic Birnessites. Clays and Clay Minerals, 2009, 57, 513-520.	1.3	71
20	Effects of Fe doping on the structures and properties of hexagonal birnessites – Comparison with Co and Ni doping. Geochimica Et Cosmochimica Acta, 2013, 117, 1-15.	3.9	71
21	Characterization of Co-doped birnessites and application for removal of lead and arsenite. Journal of Hazardous Materials, 2011, 188, 341-349.	12.4	70
22	Cadmium Removal from Aqueous Solution by a Deionization Supercapacitor with a Birnessite Electrode. ACS Applied Materials & Interfaces, 2016, 8, 34405-34413.	8.0	67
23	XPS and two-dimensional FTIR correlation analysis on the binding characteristics of humic acid onto kaolinite surface. Science of the Total Environment, 2020, 724, 138154.	8.0	67
24	Elemental Composition and Geochemical Characteristics of Iron-Manganese Nodules in Main Soils of China. Pedosphere, 2006, 16, 72-81.	4.0	66
25	Efficient catalytic As(III) oxidation on the surface of ferrihydrite in the presence of aqueous Mn(II). Water Research, 2018, 128, 92-101.	11.3	66
26	Influence of Soil Humic and Fulvic Acid on the Activity and Stability of Lysozyme and Urease. Environmental Science & Technology, 2013, 47, 5050-5056.	10.0	63
27	Factor contribution to soil organic and inorganic carbon accumulation in the Loess Plateau: Structural equation modeling. Geoderma, 2019, 352, 116-125.	5.1	62
28	Copper binding to soil fulvic and humic acids: NICA-Donnan modeling and conditional affinity spectra. Journal of Colloid and Interface Science, 2016, 473, 141-151.	9.4	59
29	Spatio-temporal dynamics of soil moisture driven by â€~Grain for Green' program on the Loess Plateau, China. Agriculture, Ecosystems and Environment, 2019, 269, 204-214.	5.3	58
30	Binding of cationic surfactants to humic substances. Colloids and Surfaces A: Physicochemical and Engineering Aspects, 2007, 306, 29-39.	4.7	57
31	Enhanced adsorption removal of arsenic from mining wastewater using birnessite under electrochemical redox reactions. Chemical Engineering Journal, 2019, 375, 122051.	12.7	54
32	Mechanisms of arsenic-containing pyrite oxidation by aqueous arsenate under anoxic conditions. Geochimica Et Cosmochimica Acta, 2017, 217, 306-319.	3.9	53
33	Effect of soil fulvic and humic acid on binding of Pb to goethite–water interface: Linear additivity and volume fractions of HS in the Stern layer. Journal of Colloid and Interface Science, 2015, 457, 121-130.	9.4	52
34	Spatial analysis of soil aggregate stability in a small catchment of the Loess Plateau, China: I. Spatial variability. Soil and Tillage Research, 2018, 179, 71-81.	5.6	50
35	High-performance Cu2+ adsorption of birnessite using electrochemically controlled redox reactions. Journal of Hazardous Materials, 2018, 354, 107-115.	12.4	50
36	A sol-gel derived pH-responsive bovine serum albumin molecularly imprinted poly(ionic liquids) on the surface of multiwall carbon nanotubes. Analytica Chimica Acta, 2016, 932, 29-40.	5.4	49

#	Article	IF	CITATIONS
37	Co2+-exchange mechanism of birnessite and its application for the removal of Pb2+ and As(III). Journal of Hazardous Materials, 2011, 196, 318-326.	12.4	48
38	Proton and Copper Binding to Humic Acids Analyzed by XAFS Spectroscopy and Isothermal Titration Calorimetry. Environmental Science & 2017, 2018, 52, 4099-4107.	10.0	48
39	Influence of Mn(III) availability on the phase transformation from layered buserite to tunnel-structured todorokite. Clays and Clay Minerals, 2008, 56, 397-403.	1.3	45
40	Effect of Soil Fulvic and Humic Acids on Pb Binding to the Goethite/Solution Interface: Ligand Charge Distribution Modeling and Speciation Distribution of Pb. Environmental Science & Technology, 2018, 52, 1348-1356.	10.0	45
41	Photochemical Formation and Transformation of Birnessite: Effects of Cations on Micromorphology and Crystal Structure. Environmental Science & amp; Technology, 2018, 52, 6864-6871.	10.0	45
42	Fourier transform infrared spectroscopy study of acid birnessites before and after Pb ²⁺ adsorption. Clay Minerals, 2012, 47, 191-204.	0.6	44
43	Enhancement of Zn2+ and Ni2+ removal performance using a deionization pseudocapacitor with nanostructured birnessite and its carbon nanotube composite electrodes. Chemical Engineering Journal, 2017, 328, 464-473.	12.7	44
44	Mechanisms on the morphology variation of hematite crystals by Al substitution: The modification of Fe and O reticular densities. Scientific Reports, 2016, 6, 35960.	3.3	43
45	High manure load reduces bacterial diversity and network complexity in a paddy soil under crop rotations. Soil Ecology Letters, 2020, 2, 104-119.	4.5	43
46	Equilibrium mono- and multicomponent adsorption models: From homogeneous ideal to heterogeneous non-ideal binding. Advances in Colloid and Interface Science, 2020, 280, 102138.	14.7	42
47	Birnessites with Different Average Manganese Oxidation States Synthesized, Characterized, and Transformed to Todorokite at Atmospheric Pressure. Clays and Clay Minerals, 2009, 57, 715-724.	1.3	41
48	Environmental significance of mineral weathering and pedogenesis of loess on the southernmost Loess Plateau, China. Geoderma, 2011, 163, 219-226.	5.1	41
49	Characteristics of micromorphology and element distribution of iron–manganese cutans in typical soils of subtropical China. Geoderma, 2008, 146, 40-47.	5.1	40
50	Mechanisms of interaction between arsenian pyrite and aqueous arsenite under anoxic and oxic conditions. Geochimica Et Cosmochimica Acta, 2018, 228, 205-219.	3.9	40
51	Proton binding to soil humic and fulvic acids: Experiments and NICA-Donnan modeling. Colloids and Surfaces A: Physicochemical and Engineering Aspects, 2013, 436, 1152-1158.	4.7	39
52	Morphology-dependent enhancement of arsenite oxidation to arsenate on birnessite-type manganese oxide. Chemical Engineering Journal, 2017, 327, 235-243.	12.7	38
53	Photochemical oxidation and dissolution of arsenopyrite in acidic solutions. Geochimica Et Cosmochimica Acta, 2018, 239, 173-185.	3.9	38
54	Transformation of Co-containing birnessite to todorokite: Effect of Co on the transformation and implications for Co mobility. Geochimica Et Cosmochimica Acta, 2019, 246, 21-40.	3.9	38

#	Article	IF	CITATIONS
55	Transformation of hydroxycarbonate green rust into crystalline iron (hydr)oxides: Influences of reaction conditions and underlying mechanisms. Chemical Geology, 2013, 351, 57-65.	3.3	36
56	Facile synthesis of birnessite-type manganese oxide nanoparticles as supercapacitor electrode materials. Journal of Colloid and Interface Science, 2016, 482, 183-192.	9.4	36
57	The Presence of Ferrihydrite Promotes Abiotic Formation of Manganese (Oxyhydr)oxides. Soil Science Society of America Journal, 2015, 79, 1297-1305.	2.2	35
58	Molecular-Scale Understanding of Sulfate Exchange from Schwertmannite by Chromate Versus Arsenate. Environmental Science & Technology, 2021, 55, 5857-5867.	10.0	35
59	Pathways of birnessite formation in alkali medium. Science in China Series D: Earth Sciences, 2005, 48, 1438-1451.	0.9	34
60	Surface adsorption and precipitation of inositol hexakisphosphate on calcite: A comparison with orthophosphate. Chemical Geology, 2016, 421, 103-111.	3.3	34
61	Solar Irradiation Induced Transformation of Ferrihydrite in the Presence of Aqueous Fe ²⁺ . Environmental Science & Technology, 2019, 53, 8854-8861.	10.0	34
62	Effect of arsenate on adsorption of Cd(II) by two variable charge soils. Chemosphere, 2007, 67, 1949-1955.	8.2	33
63	Cd2+ adsorption performance of tunnel-structured manganese oxides driven by electrochemically controlled redox. Environmental Pollution, 2019, 244, 783-791.	7.5	33
64	α-MnO2 nanowires transformed from precursor δ-MnO2 by refluxing under ambient pressure: The key role of pH and growth mechanism. Materials Chemistry and Physics, 2011, 125, 678-685.	4.0	32
65	Roles of manganese oxides in degradation of phenol under UV-Vis irradiation: Adsorption, oxidation, and photocatalysis. Journal of Environmental Sciences, 2011, 23, 1904-1910.	6.1	31
66	The simultaneous presence of glyphosate and phosphate at the goethite surface as seen by XPS, ATR-FTIR and competitive adsorption isotherms. Colloids and Surfaces A: Physicochemical and Engineering Aspects, 2016, 498, 121-127.	4.7	31
67	Effects of Al3+ doping on the structure and properties of goethite and its adsorption behavior towards phosphate. Journal of Environmental Sciences, 2016, 45, 18-27.	6.1	31
68	Local structure of Cu2+ in Cu-doped hexagonal turbostratic birnessite and Cu2+ stability under acid treatment. Chemical Geology, 2017, 466, 512-523.	3.3	31
69	Structure and properties of vanadium(V)-doped hexagonal turbostratic birnessite and its enhanced scavenging of Pb2+ from solutions. Journal of Hazardous Materials, 2015, 288, 80-88.	12.4	30
70	CD-MUSIC-EDL Modeling of Pb ²⁺ Adsorption on Birnessites: Role of Vacant and Edge Sites. Environmental Science & Technology, 2018, 52, 10522-10531.	10.0	30
71	Catalytic oxidation and adsorption of Cr(III) on iron-manganese nodules under oxic conditions. Journal of Hazardous Materials, 2020, 390, 122166.	12.4	30
72	Effects of humic acid on adhesion of Bacillus subtilis to phyllosilicates and goethite. Chemical Geology, 2015, 416, 19-27.	3.3	29

#	Article	IF	CITATIONS
73	Soil shrinkage and hydrostructural characteristics of three swelling soils in Shaanxi, China. Journal of Soils and Sediments, 2011, 11, 474-481.	3.0	28
74	Microstructure, Interaction Mechanisms, and Stability of Binary Systems Containing Goethite and Kaolinite. Soil Science Society of America Journal, 2012, 76, 389-398.	2.2	28
75	Adsorption-Desorption of Myo-Inositol Hexakisphosphate on Hematite. Soil Science, 2014, 179, 476-485.	0.9	28
76	Effects of polyphosphates and orthophosphate on the dissolution and transformation of ZnO nanoparticles. Chemosphere, 2017, 176, 255-265.	8.2	28
77	Dissolution and phase transformation processes of hausmannite in acidic aqueous systems under anoxic conditions. Chemical Geology, 2018, 487, 54-62.	3.3	28
78	Formation of Zn-Al layered double hydroxides (LDH) during the interaction of ZnO nanoparticles (NPs) with γ-Al2O3. Science of the Total Environment, 2019, 650, 1980-1987.	8.0	28
79	Quantitative and structural analysis of minerals in soil clay fractions developed under different climate zones in China by XRD with Rietveld method, and its implications for pedogenesis. Applied Clay Science, 2018, 162, 351-361.	5.2	27
80	Effects of Al substitution on local structure and morphology of lepidocrocite and its phosphate adsorption kinetics. Geochimica Et Cosmochimica Acta, 2020, 276, 109-121.	3.9	27
81	Relation of lead adsorption on birnessites with different average oxidation states of manganese and release of Mn2+/H+/K+. Journal of Environmental Sciences, 2009, 21, 520-526.	6.1	26
82	Synthetic Polymer Affinity Ligand for <i>Bacillus thuringiensis</i> (<i>Bt</i>) Cry1Ab/Ac Protein: The Use of Biomimicry Based on the <i>Bt</i> Protein–Insect Receptor Binding Mechanism. Journal of the American Chemical Society, 2018, 140, 6853-6864.	13.7	26
83	Al-substitution-induced defect sites enhance adsorption of Pb ²⁺ on hematite. Environmental Science: Nano, 2019, 6, 1323-1331.	4.3	26
84	Molecular Mechanisms of Lead Binding to Ferrihydrite–Bacteria Composites: ITC, XAFS, and μ-XRF Investigations. Environmental Science & Technology, 2020, 54, 4016-4025.	10.0	26
85	Electrochemical adsorption of cadmium and arsenic by natural Fe-Mn nodules. Journal of Hazardous Materials, 2020, 390, 122165.	12.4	26
86	Formation of todorokite from "c-disordered―H+-birnessites: the roles of average manganese oxidation state and interlayer cations. Geochemical Transactions, 2015, 16, 8.	0.7	25
87	Influence factors for the oxidation of pyrite by oxygen and birnessite in aqueous systems. Journal of Environmental Sciences, 2016, 45, 164-176.	6.1	25
88	Spatial analysis of soil aggregate stability in a small catchment of the Loess Plateau, China: II. Spatial prediction. Soil and Tillage Research, 2019, 192, 1-11.	5.6	25
89	Phosphate speciation on Al-substituted goethite: ATR-FTIR/2D-COS and CD-MUSIC modeling. Environmental Science: Nano, 2019, 6, 3625-3637.	4.3	25
90	Oxidation process of dissolvable sulfide by synthesized todorokite in aqueous systems. Journal of Hazardous Materials, 2015, 290, 106-116.	12.4	24

#	Article	IF	CITATIONS
91	Surface speciation of myo-inositol hexakisphosphate adsorbed on TiO2 nanoparticles and its impact on their colloidal stability in aqueous suspension: A comparative study with orthophosphate. Science of the Total Environment, 2016, 544, 134-142.	8.0	24
92	Lead binding to wild metal-resistant bacteria analyzed by ITC and XAFS spectroscopy. Environmental Pollution, 2019, 250, 118-126.	7.5	24
93	Quantitative analysis of Pb adsorption on sulfhydryl-modified biochar. Biochar, 2021, 3, 37-49.	12.6	24
94	Synthesis of todorokite-type manganese oxide from Cu-buserite by controlling the pH at atmospheric pressure. Microporous and Mesoporous Materials, 2009, 117, 41-47.	4.4	23
95	Large-scale size-controlled synthesis of cryptomelane-type manganese oxide OMS-2 in lateral and longitudinal directions. Journal of Materials Chemistry, 2011, 21, 5223.	6.7	23
96	Photochemical Formation Process of Schwertmannite on Montmorillonite and Corresponding Cr(VI) Adsorption Capacity. ACS Earth and Space Chemistry, 2019, 3, 718-727.	2.7	23
97	Oxidation behavior and kinetics of sulfide by synthesized manganese oxide minerals. Journal of Soils and Sediments, 2011, 11, 1323-1333.	3.0	22
98	Impact of low-molecular weight organic acids on selenite immobilization by goethite: Understanding a competitive-synergistic coupling effect and speciation transformation. Science of the Total Environment, 2019, 684, 694-704.	8.0	21
99	Effects of Reaction Conditions on the Formation of Todorokite at Atmospheric Pressure. Clays and Clay Minerals, 2006, 54, 605-615.	1.3	20
100	Role of Counteranions in Sol–Gel-Derived Alkoxyl-Functionalized Ionic-Liquid-Based Organic–Inorganic Hybrid Coatings for SPME. Chromatographia, 2012, 75, 1421-1433.	1.3	20
101	The Speciation of Cd in Cd–Fe Coprecipitates: Does Cd Substitute for Fe in Goethite Structure?. ACS Earth and Space Chemistry, 2019, 3, 2225-2236.	2.7	20
102	Adsorption and catalytic oxidation of arsenite on Fe-Mn nodules in the presence of oxygen. Chemosphere, 2020, 259, 127503.	8.2	20
103	The alkaline photo-sulfite system triggers Fe(IV/V) generation at hematite surfaces. Chemical Engineering Journal, 2020, 401, 126124.	12.7	20
104	Composition and transformation of 1.4 nm minerals in cutan and matrix of alfisols in central China. Journal of Soils and Sediments, 2007, 7, 240-246.	3.0	19
105	Synthesis of MnPO4·H2O by refluxing process at atmospheric pressure. Solid State Sciences, 2010, 12, 808-813.	3.2	19
106	The catalytic effect of AQDS as an electron shuttle on Mn(II) oxidation to birnessite on ferrihydrite at circumneutral pH. Geochimica Et Cosmochimica Acta, 2019, 247, 175-190.	3.9	19
107	Arsenic detoxification by iron-manganese nodules under electrochemically controlled redox: Mechanism and application. Journal of Hazardous Materials, 2021, 403, 123912.	12.4	19
108	Plant litter quality regulates soil eco-enzymatic stoichiometry and microbial nutrient limitation in a citrus orchard. Plant and Soil, 2021, 466, 179-191.	3.7	19

#	Article	IF	CITATIONS
109	Cobalt-doped todorokites prepared by refluxing at atmospheric pressure as cathode materials for Li batteries. Electrochimica Acta, 2010, 55, 9157-9165.	5.2	18
110	Formation and Transformation of Iron Oxide–Kaolinite Associations in the Presence of Iron(II). Soil Science Society of America Journal, 2011, 75, 45-55.	2.2	18
111	Zn sorption to biogenic bixbyite-like Mn 2 O 3 produced by Bacillus CUA isolated from soil: XAFS study with constraints on sorption mechanism. Chemical Geology, 2014, 389, 82-90.	3.3	18
112	Zinc removal from aqueous solution using a deionization pseudocapacitor with a high-performance nanostructured birnessite electrode. Environmental Science: Nano, 2017, 4, 811-823.	4.3	18
113	Symbiosis mechanism of iron and manganese oxides in oxic aqueous systems. Chemical Geology, 2018, 488, 162-170.	3.3	18
114	Mineralogical and pedogenetic evidence for palaeoenvironmental variations during the Holocene on the Loess Plateau, China. Catena, 2012, 96, 49-56.	5.0	17
115	Synthesis of hureaulite by a reflux process at ambient temperature and pressure. Microporous and Mesoporous Materials, 2012, 153, 115-123.	4.4	17
116	Interaction between lysozyme and humic acid in layer-by-layer assemblies: Effects of pH and ionic strength. Journal of Colloid and Interface Science, 2014, 430, 40-46.	9.4	17
117	Facile crystal-structure-controlled synthesis of iron oxides for adsorbents and anode materials of lithium batteries. Materials Chemistry and Physics, 2016, 170, 239-245.	4.0	17
118	Roles of different types of oxalate surface complexes in dissolution process of ferrihydrite aggregates. Scientific Reports, 2018, 8, 2060.	3.3	17
119	Effects of Co(II) ion exchange, Ni(II)- and V(V)-doping on the transformation behaviors of Cr(III) on hexagonal turbostratic birnessite-water interfaces. Environmental Pollution, 2020, 256, 113462.	7.5	17
120	Highly enhanced oxidation of arsenite at the surface of birnessite in the presence of pyrophosphate and the underlying reaction mechanisms. Water Research, 2020, 187, 116420.	11.3	17
121	Arsenic release from arsenopyrite oxidative dissolution in the presence of citrate under UV irradiation. Science of the Total Environment, 2020, 726, 138429.	8.0	17
122	Quantitative Characterization of the Site Density and the Charged State of Functional Groups on Biochar. ACS Sustainable Chemistry and Engineering, 2021, 9, 2600-2608.	6.7	17
123	Investigation on electrochemical reduction process of Nb2O5 powder in molten CaCl2 with metallic cavity electrode. Electrochimica Acta, 2008, 53, 4074-4081.	5.2	16
124	Aging promotes todorokite formation from layered manganese oxide at near-surface conditions. Journal of Soils and Sediments, 2010, 10, 1540-1547.	3.0	16
125	One-step synthesis of sea urchin-like α-MnO2 using KIO4 as the oxidant and its oxidation of arsenite. Materials Letters, 2012, 77, 60-62.	2.6	16
126	Mixed ad/desorption kinetics unraveled with the equilibrium adsorption isotherm. Colloids and Surfaces A: Physicochemical and Engineering Aspects, 2019, 577, 709-722.	4.7	16

#	Article	IF	CITATIONS
127	Adsorption and precipitation of <i>myo</i> â€inositol hexakisphosphate onto kaolinite. European Journal of Soil Science, 2020, 71, 226-235.	3.9	16
128	Intrinsic mechanisms of calcium sulfite activation by siderite for atrazine degradation. Chemical Engineering Journal, 2021, 426, 131917.	12.7	16
129	Structural Controls on the Catalytic Polymerization of Hydroquinone by Birnessites. Clays and Clay Minerals, 2011, 59, 525-537.	1.3	15
130	SoilChip-XPS integrated technique to study formation of soil biogeochemical interfaces. Soil Biology and Biochemistry, 2017, 113, 71-79.	8.8	15
131	Effects of <i>Myo</i> -inositol Hexakisphosphate on Zn(II) Sorption on γ-Alumina: A Mechanistic Study. ACS Earth and Space Chemistry, 2018, 2, 787-796.	2.7	15
132	Suppressed phosphorus-mineralizing bacteria after three decades of fertilization. Agriculture, Ecosystems and Environment, 2022, 323, 107679.	5.3	15
133	XAFS studies on surface coordination of Pb2+ on birnessites with different average oxidation states. Colloids and Surfaces A: Physicochemical and Engineering Aspects, 2011, 379, 86-92.	4.7	14
134	Catalytic oxidation of arsenite and reaction pathways on the surface of CuO nanoparticles at a wide range of pHs. Geochemical Transactions, 2018, 19, 12.	0.7	14
135	Effects of Mn ²⁺ , Ni ²⁺ , and Cu ²⁺ on the Formation and Transformation of Hydrosulfate Green Rust: Reaction Processes and Underlying Mechanisms. ACS Earth and Space Chemistry, 2019, 3, 519-530.	2.7	14
136	Preference of Co over Al for substitution of Fe in goethite (α-FeOOH) structure: Mechanism revealed from EXAFS, XPS, DFT and linear free energy correlation model. Chemical Geology, 2020, 532, 119378.	3.3	14
137	High-efficiency As(III) oxidation and electrocoagulation removal using hematite with a chargeâ~'discharge technique. Science of the Total Environment, 2020, 703, 135678.	8.0	14
138	Sequestration of heavy metals in soil aggregates induced by glomalin-related soil protein: A five-year phytoremediation field study. Journal of Hazardous Materials, 2022, 437, 129445.	12.4	14
139	Abiotic photomineralization and transformation of iron oxide nanominerals in aqueous systems. Environmental Science: Nano, 2018, 5, 1169-1178.	4.3	13
140	Short-term effect of manure and straw application on bacterial and fungal community compositions and abundances in an acidic paddy soil. Journal of Soils and Sediments, 2021, 21, 3057-3071.	3.0	13
141	Disentangling drivers of soil microbial nutrient limitation in intensive agricultural and natural ecosystems. Science of the Total Environment, 2022, 806, 150555.	8.0	13
142	Geochemical characteristics of selected elements in iron–manganese cutans and matrices of Alfisols in central China. Journal of Geochemical Exploration, 2009, 103, 30-36.	3.2	12
143	Influence of lysozyme complexation with purified Aldrich humic acid on lysozyme activity. European Journal of Soil Science, 2012, 63, 550-557.	3.9	12
144	Effect of 1-1 electrolyte concentration on the adsorption/desorption of copper ion on synthetic birnessite. Journal of Soils and Sediments, 2010, 10, 879-885.	3.0	11

#	Article	IF	CITATIONS
145	Synthesis of a Nanofibrous Manganese Oxide Octahedral Molecular Sieve with Co(NH ₃) ₆ 3+ Complex Ions as a Template via a Reflux Method. Crystal Growth and Design, 2010, 10, 3355-3362.	3.0	11
146	Enhanced oxidation of arsenite to arsenate using tunable K+ concentration in the OMS-2 tunnel. Environmental Pollution, 2018, 238, 524-531.	7.5	11
147	Influence of humic acid on transport, deposition and activity of lysozyme in quartz sand. Environmental Pollution, 2018, 242, 298-306.	7.5	11
148	Effects of myo-inositol hexakisphosphate, ferrihydrite coating, ionic strength and pH on the transport of TiO2 nanoparticles in quartz sand. Environmental Pollution, 2019, 252, 1193-1201.	7.5	11
149	Synergistic adsorption of Cd(II) and As(V) on birnessite under electrochemical control. Chemosphere, 2020, 247, 125822.	8.2	11
150	Effects of aluminum substitution on the surface charge of colloidal goethite particles: experiments and MUSIC modeling. Environmental Science and Pollution Research, 2020, 27, 38397-38406.	5.3	11
151	Microstructure of Al-substituted goethite and its adsorption performance for Pb(II) and As(V). Science of the Total Environment, 2021, 790, 148202.	8.0	11
152	Insights into the improving mechanism of defect-mediated As(V) adsorption on hematite nanoplates. Chemosphere, 2021, 280, 130597.	8.2	11
153	Factors governing formation of todorokite at atmospheric pressure. Science in China Series D: Earth Sciences, 2005, 48, 1678-1689.	0.9	10
154	Factors Governing the Formation of Lithiophorite at Atmospheric Pressure. Clays and Clay Minerals, 2009, 57, 353-360.	1.3	10
155	Profile distribution of soil organic and inorganic carbon following revegetation on the Loess Plateau, China. Environmental Science and Pollution Research, 2018, 25, 30301-30314.	5.3	10
156	Selective adsorption of soil humic acid on binary systems containing kaolinite and goethite: Assessment of sorbent interactions. European Journal of Soil Science, 2019, 70, 1098-1107.	3.9	10
157	Coupled morphological and structural evolution of δ-MnO ₂ to α-MnO ₂ through multistage oriented assembly processes: the role of Mn(<scp>iii</scp>). Environmental Science: Nano, 2020, 7, 238-249.	4.3	10
158	Synthesis of todorokite by refluxing process and its primary characteristics. Science in China Series D: Earth Sciences, 2004, 47, 760-768.	0.9	9
159	Formation and Morphology Evolution from Ferrihydrite to Hematite in the Presence of Tartaric Acid. ACS Earth and Space Chemistry, 2019, 3, 562-570.	2.7	9
160	Formation and transformation of manganese(III) intermediates in the photochemical generation of manganese(IV) oxide minerals. Chemosphere, 2021, 262, 128082.	8.2	9
161	Highly efficient removal of Cu-organic chelate complexes by flow-electrode capacitive deionization-self enhanced oxidation (FCDI-SEO): Dissociation, migration and degradation. Chemical Engineering Journal, 2022, 445, 136811.	12.7	9
162	Effects of myo-inositol hexakisphosphate and orthophosphate adsorption on aggregation of CeO2 nanoparticles: roles of pH and surface coverage. Environmental Chemistry, 2016, 13, 34.	1.5	8

#	Article	IF	CITATIONS
163	Oxidation and Catalytic Oxidation of Dissolved Sulfide By Manganite in Aqueous Systems. Clays and Clay Minerals, 2017, 65, 299-309.	1.3	8
164	Effect of citrate on the species and levels of Al impurities in ferrihydrite. Colloids and Surfaces A: Physicochemical and Engineering Aspects, 2018, 539, 140-147.	4.7	8
165	Effect of Cd and Al Coincorporation on the Structures and Properties of Goethite. ACS Earth and Space Chemistry, 2018, 2, 1283-1293.	2.7	8
166	Effective Zinc Adsorption Driven by Electrochemical Redox Reactions of Birnessite Nanosheets Generated by Solar Photochemistry. ACS Sustainable Chemistry and Engineering, 2018, 6, 13907-13914.	6.7	8
167	Interaction mechanism of dissolved Cr(VI) and manganite in the presence of goethite coating. Environmental Pollution, 2020, 260, 114046.	7.5	8
168	Exploring the effects of landscape structure on aerosol optical depth (AOD) patterns using GIS and HJ-1B images. Environmental Sciences: Processes and Impacts, 2016, 18, 265-276.	3.5	7
169	Desorption rate of glyphosate from goethite as affected by different entering ligands: hints on the desorption mechanism. Environmental Chemistry, 2017, 14, 288.	1.5	7
170	Conformational modifications of lysozyme caused by interaction with humic acid studied with spectroscopy. Science of the Total Environment, 2021, 768, 144858.	8.0	7
171	Characteristics of the fifth paleosol complex (S5) in the southernmost part of the Chinese Loess Plateau and its paleo-environmental significance. Catena, 2014, 122, 130-139.	5.0	6
172	Absorption mechanisms of Cu2+ on a biogenic bixbyite-like Mn2O3 produced by Bacillus CUA isolated from soil. Geochemical Transactions, 2015, 16, 5.	0.7	6
173	Interaction mechanism and kinetics of ferrous sulfide and manganese oxides in aqueous system. Journal of Soils and Sediments, 2018, 18, 564-575.	3.0	6
174	Resolving humic and fulvic acids in binary systems influenced by adsorptive fractionation to Fe-(hydr)oxide with focus on UV–Vis analysis. Chemical Engineering Journal, 2020, 389, 124380.	12.7	6
175	Facet-dependent surface charge and Pb2+ adsorption characteristics of hematite nanoparticles: CD-MUSIC-eSGC modeling. Environmental Research, 2021, 196, 110383.	7.5	6
176	Epitaxial growth mechanism of heterogeneous catalytic oxidation of Mn(II) on manganite under oxic conditions. Chemical Geology, 2020, 547, 119670.	3.3	6
177	Structural-controlled formation of nano-particle hematite and their removal performance for heavy metal ions: A review. Chemosphere, 2022, 306, 135540.	8.2	6
178	Effect of carbonate and phosphate ratios on the transformation of calcium orthophosphates. Materials Research Bulletin, 2014, 55, 114-120.	5.2	5
179	The distinct effects of isomorphous substitution of various divalence trace metals on hematite structure. Materials Chemistry and Physics, 2018, 217, 40-47.	4.0	5
180	Photoinduced Self-Organized Precipitation in Leachate for Remediation of Heavy Metal Contaminated Soils. ACS ES&T Engineering, 2022, 2, 1376-1385.	7.6	5

#	Article	IF	CITATIONS
181	Characteristics of Iron-Manganese Cutans and Matrices in Alfisols and Ultisols of Subtropical China. Soil Science, 2009, 174, 238-246.	0.9	4
182	Factors Influencing the Elemental Distribution in Iron-Manganese Cutans of Three Subtropical Soils. Soil Science, 2011, 176, 48-56.	0.9	4
183	Transformation from Phyllomanganates to Todorokite under Various Conditions: A Review of Implication for Formation Pathway of Natural Todorokite. ACS Symposium Series, 2015, , 107-134.	0.5	4
184	Goethite effects on transport and activity of lysozyme with humic acid in quartz sand. Colloids and Surfaces A: Physicochemical and Engineering Aspects, 2020, 604, 125319.	4.7	4
185	Influences and Mechanisms of As(V) Concentration and Environmental Factors on Hydrosulfate Green Rust Transformation. Acta Chimica Sinica, 2017, 75, 608.	1.4	4
186	Regional differences in mineral weathering characteristics of zonal soils under intensive agriculture. Applied Clay Science, 2021, 215, 106336.	5.2	4
187	Effect of humic acid on lysozyme interaction with montmorillonite and kaolinite. Science of the Total Environment, 2022, 834, 155370.	8.0	4
188	Shapeâ€controlled Synthesis of Nanostructure Ramsdelliteâ€ŧype Manganese Oxide at Atmospheric Pressure. Chinese Journal of Chemistry, 2010, 28, 2301-2307.	4.9	3
189	In situ detection of intermediates from the interaction of dissolved sulfide and manganese oxides with a platinum electrode in aqueous systems. Environmental Chemistry, 2017, 14, 178.	1.5	3
190	Origin of Smectite in Salinized Soil of Junggar Basin in Xinjiang of China. Minerals (Basel,) Tj ETQq0 0 0 rgBT /Ove	erlock 10 7 2.0	rf 50 382 Td
191	Quantitative investigation of ZnO nanoparticle dissolution in the presence of δ-MnO2. Environmental Science and Pollution Research, 2020, 27, 14751-14762.	5.3	3
192	Abiotic Synthetic Antibodies to Target a Specific Protein Domain and Inhibit Its Function. ACS Applied Materials & Interfaces, 2022, , .	8.0	3
193	Distribution, Species and Interfacial Reactions of Phytic Acid in Environment. Ying Yong Yu Huan Jing Sheng Wu Xue Bao = Chinese Journal of Applied and Environmental Biology, 2012, 18, 494.	0.1	2
194	Spectroscopic investigation of conformational changes in urease caused by interaction with humic acid. Colloids and Surfaces B: Biointerfaces, 2022, 215, 112510.	5.0	2
195	Prediction and analysis of the soil organic matter distribution with the spatiotemporal kriging method. Earth Science Informatics, 0, , .	3.2	2
196	Effect and fate of Ni during aging and thermal-induced phyllomanganate-to-tectomanganate transformation. Geochimica Et Cosmochimica Acta, 2022, 333, 200-215.	3.9	2
197	Microcalorimetric Study on the Growth and Metabolism of a Manganese-Oxidizing Bacterium and its Mutant Strain. Geomicrobiology Journal, 2015, 32, 585-593.	2.0	1
198	Influence of reduction on the fluorescent units and proton binding of humic acids: Synchronous fluorescence spectrum and NICA-Donnan modeling. Colloids and Surfaces A: Physicochemical and Engineering Aspects, 2021, 626, 127000.	4.7	1

#	Article	IF	CITATIONS
199	Contribution of Soil Active Components to the Control of Heavy Metal Speciation. , 2018, , 165-188.		Ο
200	Mechanisms of efficient As(III) and As(V) removal by Ni-coprecipitated hausmannite nanocomposites. Journal of Environmental Chemical Engineering, 2022, 10, 107684.	6.7	0